

FINITE ELEMENT ANALYSIS OF STRAIN NON-UNIFORMITY IN TWO PROCESSES OF SEVERE PLASTIC DEFORMATION

J. M a c i e j e w s k i, H. K o p e ć, H. P e t r y k

Institute of Fundamental Technological Research
Polish Academy of Sciences
Warsaw, Poland

Two severe plastic deformation (SPD) processing techniques, namely equal-channel angular pressing (ECAP) and cyclic extrusion-compression (CEC), are investigated by using the finite element method. The major aspect examined is the non-uniformity of the accumulated, equivalent plastic strain after processing with the use of different shapes of the die. The quantitative effect of several parameters on the plastic flow is determined. It is found that the diameter ratio of the chambers and narrower channel in the CEC method, and also the inclination angle of connecting conical parts, can affect strongly the degree of strain non-uniformity. Comparison is made of distributions of equivalent strain after two passes of ECAP for two different routes and with two die profiles.

1. INTRODUCTION

In the last two decades many studies have been devoted to the material processing by applying severe plastic deformation (SPD). The principal aim of imposing extremely large plastic strains is to achieve ultra-fine grain sizes. Decrease of grain size to a sub-micrometer level is related to beneficial mechanical properties such as very high strength which may also be accompanied by low-temperature superplasticity. In contradistinction to traditional cold rolling or extrusion, the purpose of SPD is not to reduce a cross-section dimension to a given value. Several SPD processes have been designed so that the billet shape remains essentially unchanged after the processing by cyclic deformation. Two such processes are investigated here, namely, equal-channel angular pressing (ECAP) and cyclic extrusion-compression (CEC). ECAP is the most popular SPD technique, introduced in the former Soviet Union [1]. An extensive review of the vast literature and recent developments related to the use of ECAP for grain refinement can be found in Ref. [2]. CEC is the SPD technique developed in Poland [3] and subsequently studied in a series of papers, e.g. [4–7].

Majority of papers dealing with SPD techniques have concentrated on microstructural aspects of the grain refinement and on the changes in mechanical prop-

erties of the material. Modelling of the material flow was also performed by using an analytic approach [8–10], the slip-line field theory [11, 12], an upper-bound approach [13, 14], and the finite element method (FEM) [15–23], predominantly for ECAP. The present authors are aware of the only one finite element study of the CEC process [17].

The aim of this paper is to present selected results of FEM simulations of the above-mentioned two SPD processes. The axisymmetric FEM simulations of CEC and plane-strain simulations of ECAP have been performed by using the commercial computer code ADINA [24]. The modelling of CEC constitutes the major part of this work and provides new results. ECAP was thoroughly studied in the literature, nevertheless the present analysis of two passes for two different ECAP routes and two die profiles and for different friction conditions, appears to be novel. The major aspect examined below is the non-uniformity of the accumulated, equivalent plastic strain after processing with the use of different shapes of the die. The predictions of numerical simulations can help in optimal design of the tools for technological applications.

2. SIMULATIONS OF CYCLIC EXTRUSION-COMPRESSION (CEC)

2.1. Description

The cyclic extrusion-compression method can be applied to achieve unlimited accumulated strains by a combination of the processes of extrusion and compression, with preservation of the initial shape of a material sample [3–7]. This is an important advantage of the CEC method. The sample (Fig. 1) is placed in the die consisting of left and right chambers of equal diameter d_0 , connected by a channel of a smaller diameter d_m . The deformation proceeds by the cyclic flow of metal from one chamber to the other. For example, in a single cycle the sample is extruded from the left chamber, say, by the left active punch, with the backpressure exerted by the right passive punch which causes plastic compression of the material just after extrusion. In the next cycle, the right punch becomes active and the deformation proceeds by flow of the sample from the

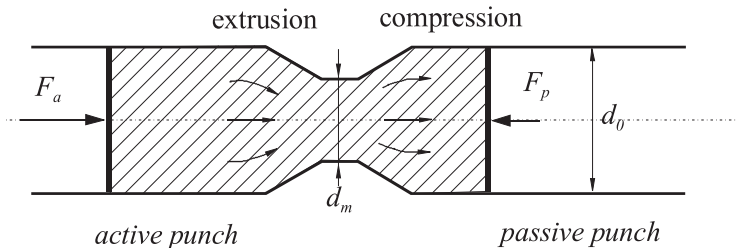


FIG. 1. Sketch of CEC deformation process.

right chamber to the left, and so on. In this way the metal sample is deformed cyclically to unlimited strains without removing the material sample from the apparatus. If the deformation is assumed to be uniform, then the magnitude of the accumulated equivalent (von Mises) strain after n deformation cycles can be estimated as follows [3]:

$$(2.1) \quad \varepsilon = 4n \ln \left(\frac{d_0}{d_m} \right).$$

The FEM simulations of the CEC process were performed using the ADINA 8.3 System, assuming axisymmetric deformation and large strain and large displacement kinematics under isothermal and quasistatic conditions. A finite element mesh covering the deformed material consisted of 2240 axisymmetric 9-node solid elements. The die and the punches were modelled as rigid bodies. Figure 2 presents the scheme of the FE mesh and of the die shape. In the numerical analysis the die shape was described by parameters: d_0 , d_m , α (inclination angle of the conical parts) and a (length of the central cylindrical channel). The transition from the cylindrical to conical parts of the die was modelled as a curve of radius $R = 1/2 (d_0 - d_m)$.

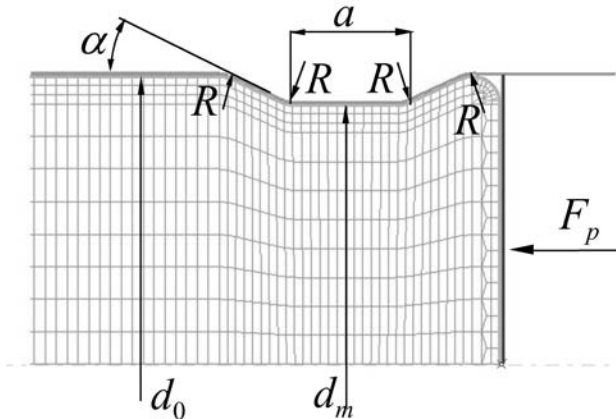


FIG. 2. Scheme of the finite element mesh and CEC channel geometry.

In the calculations the material was modelled as elastic-plastic with isotropic hardening described by a multilinear approximation of a true (logarithmic) strain – true (Cauchy) stress curve shown in Fig. 3. The experimental data points that correspond to polycrystalline pure aluminium (99.99%) deformed at room temperature (293 K) in a wide range of strain are taken from Refs. [25]. The experimental data for low strain level were obtained in the tension test, whereas for larger strains the data were reported for samples produced in the ECAP process [26, 27]. The elasticity parameters were taken as Young's modulus $E = 70$ GPa and Poisson's ratio $\nu = 0.32$.

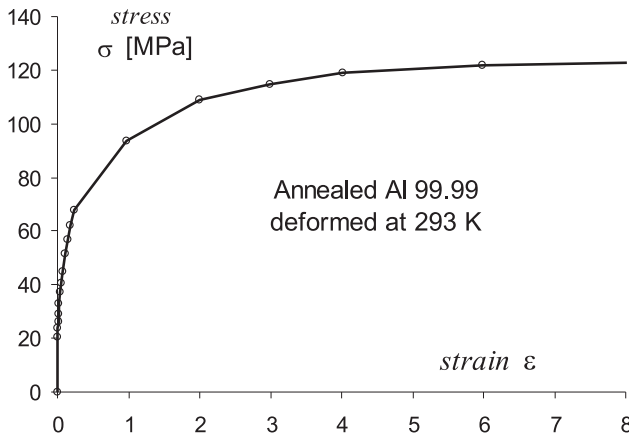


FIG. 3. Experimental data points [25–27] and a multilinear approximation of the true stress–true strain curve for a wide range of strain for pure Al deformed at room temperature (293 K).

In the real CEC process the samples were covered with a graphite lubricant before the deformation process [5]. In the calculation, the frictionless contact as well as the nonlinear friction model were used. The nonlinear friction law was assumed in the form

$$(2.2) \quad \tau_n = A_1 (1 - \exp(-\sigma_n A_2)),$$

where τ_n, σ_n are the shear and normal contact stress components, respectively, and A_1, A_2 are the friction parameters whose meaning is indicated in Fig. 4.

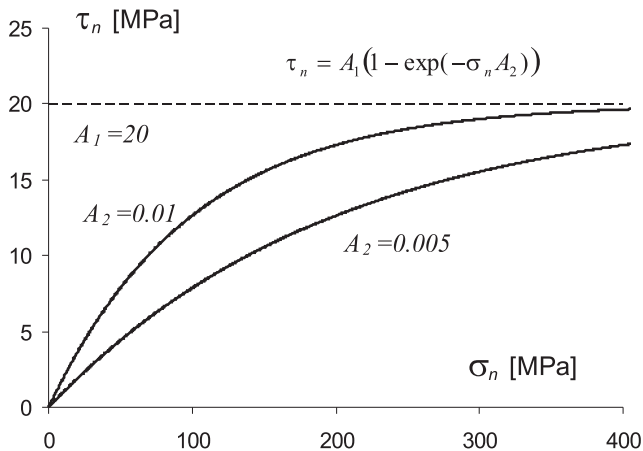


FIG. 4. The nonlinear friction law used in numerical simulations.

Two different sequences of calculation of the CEC process have been used (Fig. 5). In the first sequence illustrated in Fig. 5a, the material was initially in the left chamber only. As the left punch was kinematically forced to move, the forward extrusion (without the passive punch) was executed. Next the pressure was applied to the right punch, aimed at complete filling of the die space, while the active left punch was still moving. As a result, a roughly uniform deformation zone around the sample axis in the central part was obtained. In the end zone of the sample the strain distribution was non-uniform. In the second sequence of calculation, the initial material position was as shown in Fig. 5b. The right-hand side of the sample was positioned at once beyond the narrower channel, the hardening effect of compression by the right-hand punch being neglected. Then, along with the active left punch motion, the backpressure was exerted by the right punch. After completing the first cycle of deformation, the resulting strain distributions were found to be of steady-state type and practically the same for both calculation sequences, except in the vicinity of the right end of the sample. Therefore, in further calculations only the second sequence was used as a simpler approach.

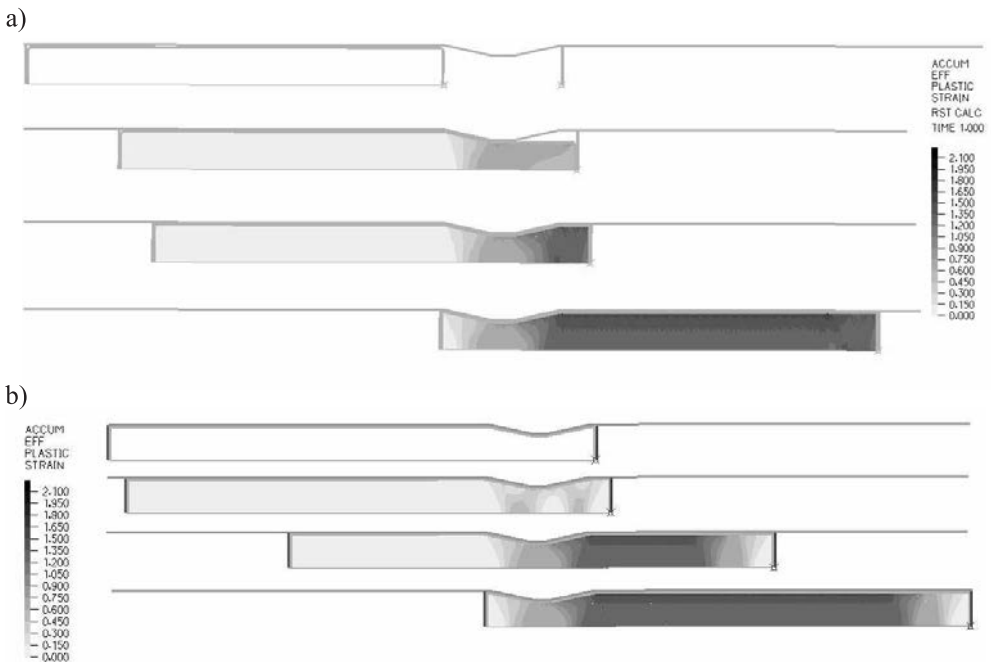


FIG. 5. Equivalent plastic strain field in the subsequent phases of the first pass in CEC process for two different sequences of calculation: a) initial position of the sample in the left chamber only, b) initial position of the sample covers the central channel.

2.2. Results and discussion

Figure 6 shows the distribution of accumulated equivalent plastic strain in the transverse cross-section of the sample after the first cycle of the CEC process for different diameter ratios $d_0/d_m = 15/11, 10/8, 10/9, 10/9.5$. The results were taken from for the major (central) part of the sample where the strain was uniform along the axis. In this calculation, a frictionless contact was assumed and the additional shape parameters were: inclination angle of conical parts $\alpha = 25^\circ$ and channel length $a = 2$ mm. The dashed lines in the figure represent the theoretical magnitude of accumulated equivalent plastic strain after one cycle which, according to Eq. (2.1), is equal to 1.24, 0.982, 0.421, 0.20 for diameter ratio $d_0/d_m = 15/11, 10/8, 10/9, 10/9.5$, respectively. It is clearly seen that the deformation is non-uniform with the peak near the outer radius of the sample, with a strong influence of the diameter ratio on the strain non-uniformity. For the dies with diameter ratio 10/9 and 10/9.5, the accumulated equivalent strain near the sample axis is less than the theoretical value. The strain distribution is fairly uniform for $d_0/d_m = 15/11$.

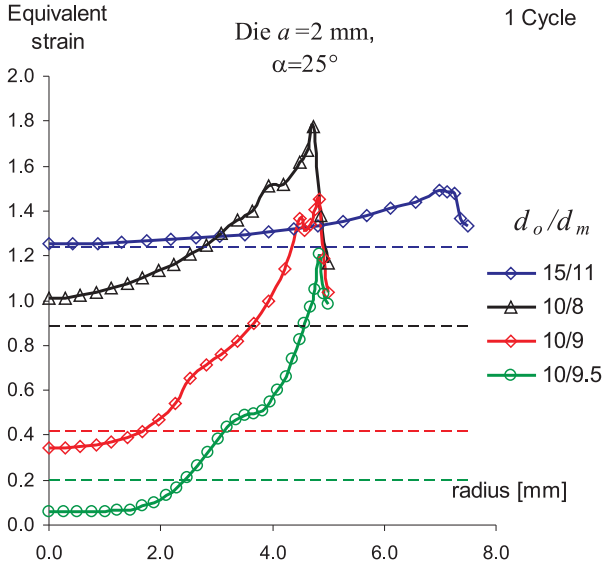


FIG. 6. Accumulated equivalent plastic strain versus the sample radius after one cycle of the CEC process, with different diameter ratios $d_0/d_m = 15/11, 10/8, 10/9, 10/9.5$. Channel length $a = 2$ mm, inclination angle of conical parts $\alpha = 25^\circ$, frictionless conditions.

The angle of inclination of conical parts of the die has also a significant influence on the resulting homogeneity of the sample. The variation of accumulated equivalent plastic strain with respect to the sample radius for different inclina-

tion angles $\alpha = 15^\circ, 25^\circ, 35^\circ, 45^\circ$ is presented in Fig. 7. These calculations were performed for diameter ratio $d_0/d_m = 10/8$ and channel length $a = 2$ mm. With the angle growth, the non-homogeneity increases.

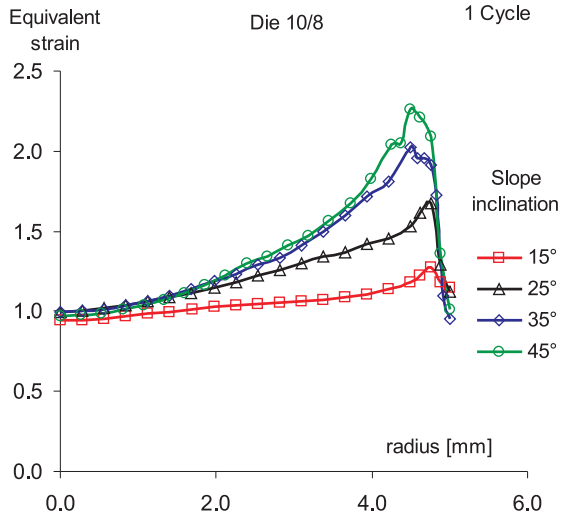


FIG. 7. Accumulated equivalent plastic strain versus the sample radius after one cycle of the CEC process, with $d_0/d_m = 10/8$ and channel length $a = 2$ mm, for different inclination angles $\alpha = 15^\circ, 25^\circ, 35^\circ, 45^\circ$ of conical parts of the die.

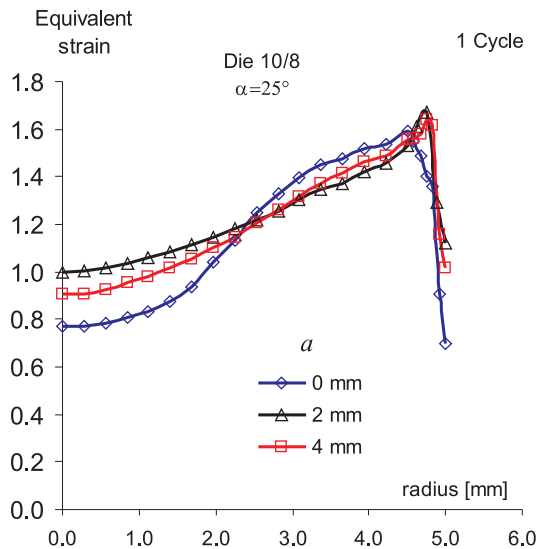


FIG. 8. Accumulated equivalent plastic strain versus the sample radius after 1 cycle of the CEC process, with $d_0/d_m = 10/8$ and $\alpha = 25^\circ$, for different channel lengths $a = 0, 2, 4$ mm.

The influence of the length a of the cylindrical channel of the die is less substantial as that shown in Fig. 8. The non-homogeneity is the largest for channel length $a = 0$ when the conical parts of the die are in contact.

Figure 9 shows the effect of friction on the material/tool contact surface, on the radial distribution of accumulated equivalent plastic strain. In the case of diameter ratio 10/9 and inclination angle of conical parts $\alpha = 25^\circ$, the influence of friction was significant only near the outer surface being in contact with the tool, whereas in the remaining part the deformation was only slightly affected by friction.

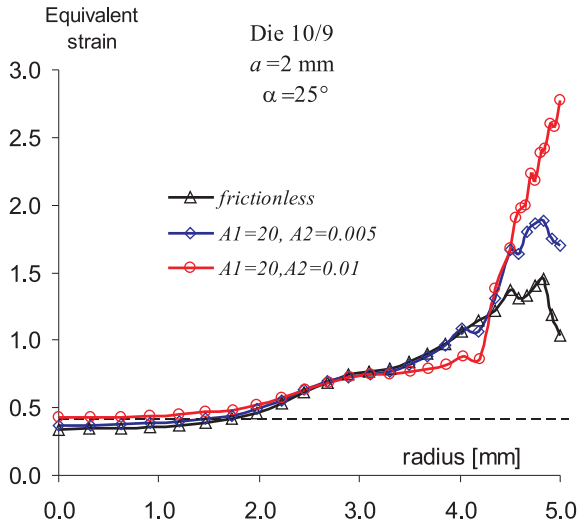


FIG. 9. Accumulated equivalent plastic strain distribution for different friction parameters.

The next three figures show perhaps the most important effect of the ratio of the chamber and channel diameters on the plastic strain non-uniformity. Each figure corresponds to the same values of channel length and inclination angle of conical parts, taken in this case as $a = 2$ mm and $\alpha = 25^\circ$, respectively, while the diameter ratio is the only variable parameter. Frictionless contact has been assumed. In Fig. 10 the radial distribution of the accumulated equivalent plastic strain is shown after the first, second and third cycle of CEC, for diameter ratio 10/8. The distribution is clearly not uniform, but the degree of non-uniformity (ratio of maximum to minimum equivalent strains) equal to 1.7 does not increase after subsequent cycles. Therefore, in the range of severe plastic deformation where the strain hardening saturates, that strain non-uniformity does not need to lead to substantial macroscopic heterogeneity in the mechanical properties such as the yield stress or microhardness. In fact, the microhardness distributions

along the sample diameter, after 4 and 22 cycles of CEC with the die of diameter, ratio 10/8, were found to be fairly uniform and close to each other [3].

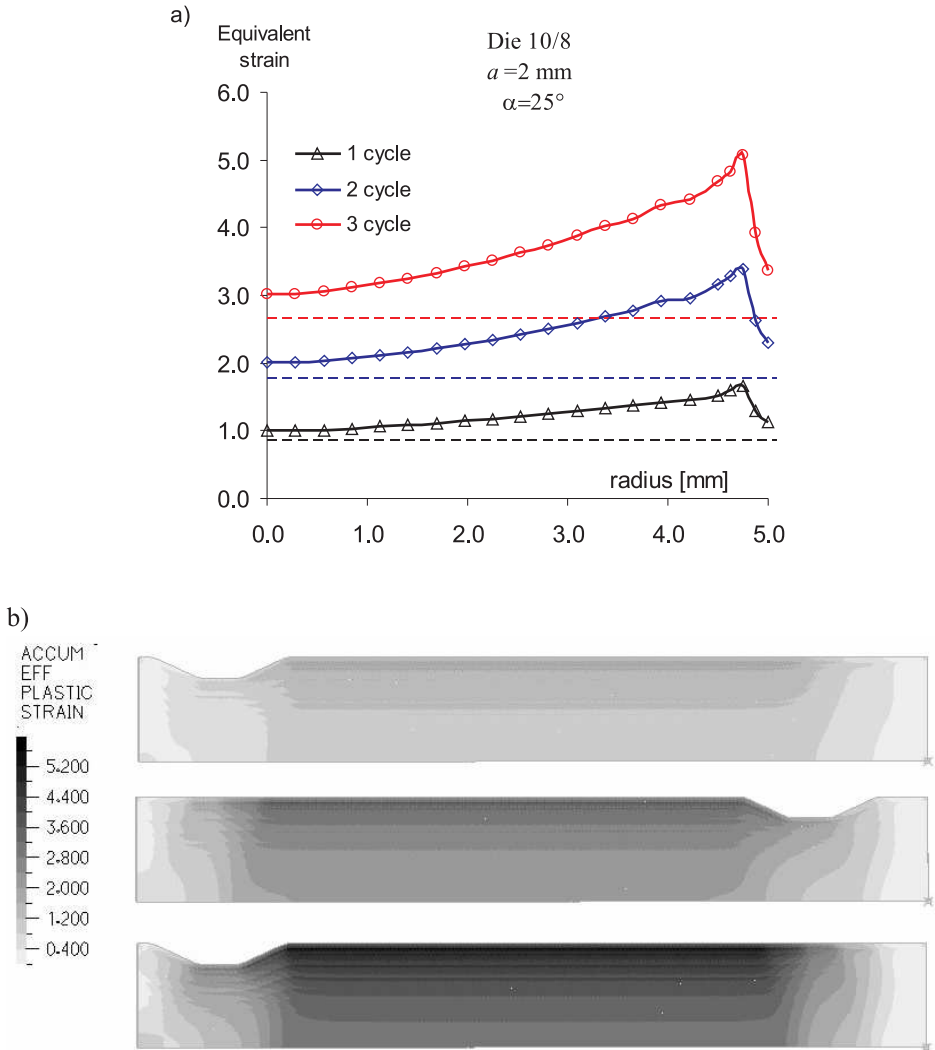


FIG. 10. Accumulated equivalent plastic strain after 1, 2 and 3 cycles of the CEC process, with $d_0/d_m = 10/8$, $a = 2 \text{ mm}$ and $\alpha = 25^\circ$; a) distribution versus the sample radius, b) 2D distribution in the longitudinal cross-section.

The situation changes when the difference in diameter of the chambers and the connecting channel is too small. As shown in Figs. 11 and 12, in that case the degree of non-uniformity is large and increases with subsequent cycles to 9.7 and 40, for the diameter ratio $d_0/d_m = 10/9$ and $10/9.5$, respectively. The

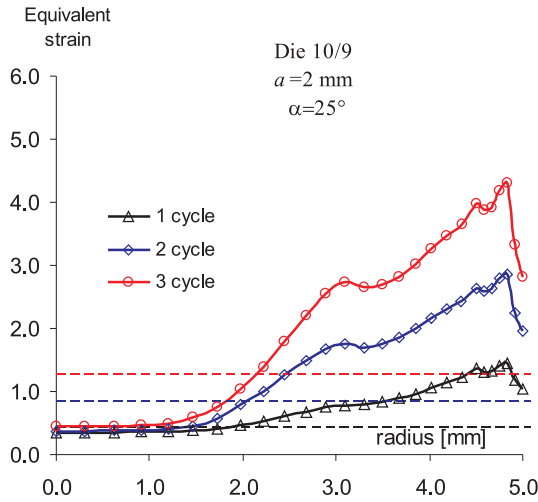


FIG. 11. Accumulated equivalent plastic strain versus the sample radius after 1, 2 and 3 cycles of the CEC process, with $d_0/d_m = 10/9$.

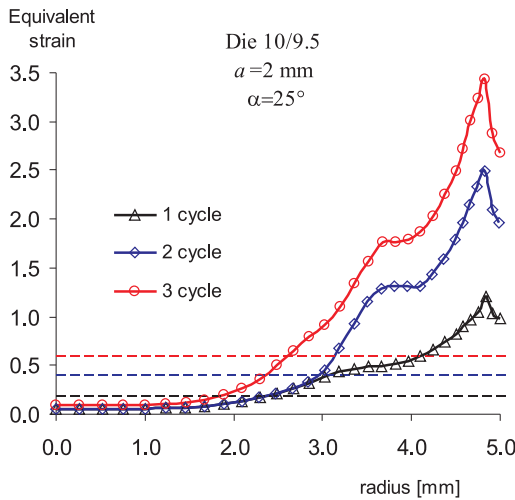


FIG. 12. Accumulated equivalent plastic strain versus the sample radius after 1, 2 and 3 cycles of CEC, with $d_0/d_m = 10/9.5$.

equivalent strain in the inner part of the sample, deformed when using the die of diameter ratio $d_0/d_m = 10/9$ is accumulated much slower than that predicted by the formula (2.1) for uniform distribution of strain, while in the outer part it becomes much larger. If the diameter ratio d_0/d_m is smaller, then the plastic strain accumulation in the inner part may even be suspended, cf. Fig. 12.

It may be noted that the above conclusion has been drawn from the numerical results obtained by using the conventional plasticity model, which does not describe the formation of macroscopic shear bands. Such bands running across the sample were observed experimentally [4, 6]. Presence of macroscopic shear bands, while introducing local flow non-uniformities, might nevertheless reduce the strain non-uniformity on the scale of the sample radius. This question requires further study which is, however, beyond the scope of the present paper.

3. SIMULATIONS OF EQUAL-CHANNEL ANGULAR PRESSING (ECAP)

3.1. Description

The ECAP process was analyzed much more frequently in the literature than CEC, therefore some results for ECAP are presented here to provide a comparison of the flow non-uniformity in both processes. As it is well known [2], the nature of the deformation imposed by ECAP is simple shear which occurs as the sample passes through an abruptly bent channel. The square cross-sectional dimensions do not experience any changes, therefore the sample may be pressed repeatedly to achieve very high accumulated strains. Different deformation routes are possible here. As illustrated in Fig. 13, the billet can be placed again in the die without any rotation about its axis (route A), or be rotated by 180° after each pass (route C). This is equivalent to pressing the sample through an *U*-shaped or *S*-shaped channel, respectively; this analogy has been used in the present 2D calculations. Other routes (B_A – the billet is rotated clockwise through 90° between each cycle, B_C – the billet is rotated through 90° clockwise

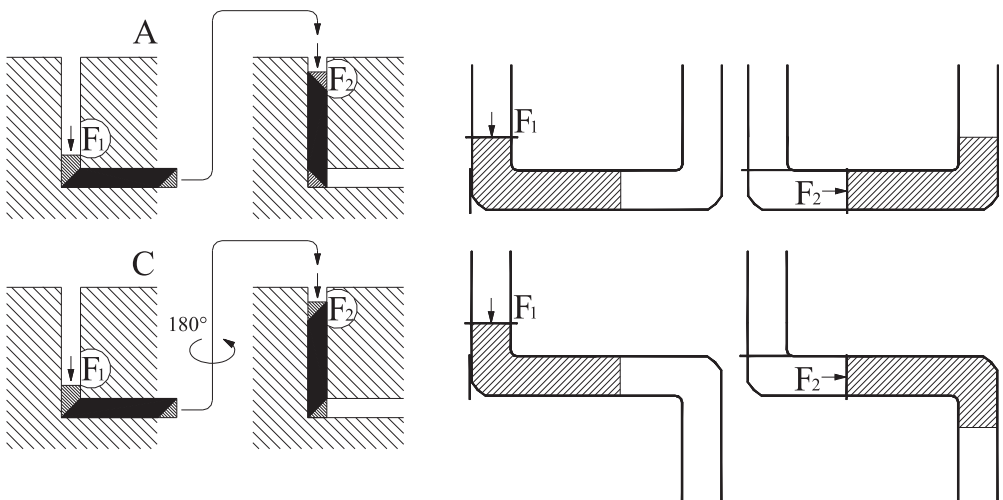


FIG. 13. Sketch of the examined routes of ECAP.

and then 90° anticlockwise each alternate cycle) are not examined here since they would require a more complex 3D analysis.

Details of die geometry have a certain influence of the material flow through the die. In this paper, two types of die geometry have been investigated, as shown in Fig. 14. Such dies with the angle of intersection of the channels equal to $\phi = 90^\circ$ and with the angle of the outer arc of curvature where the two channels intersect, equal either to $\psi = 20^\circ$ or $\psi = 0^\circ$, are typical in applications [2]. The radius r of rounded-off corners is introduced here mainly to overcome numerical problems related to simulation of plastic flow around sharp corners. The finite element mesh consisted of 5472 plane-strain 9-node elements; its part is shown in Fig. 15.

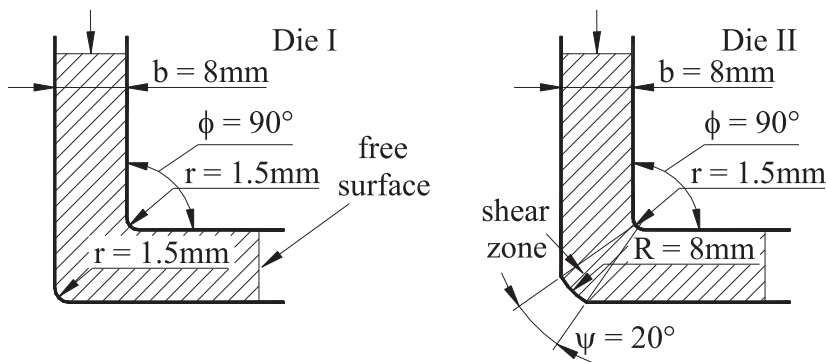


FIG. 14. Geometry of two ECAP dies used in numerical simulations.

The material model used in calculations corresponds to pure aluminium as in CEC calculations, however, with two modifications. First, hardening was described here in a more simple way by assuming linear hardening from the initial yield stress $\sigma_0 = 95$ [MPa] with the tangent modulus $E_T = 15$ [MPa]. Either pure isotropic or pure kinematic hardening were examined.

3.2. FEM results and discussion

Figure 15 shows the distribution of the accumulated equivalent plastic strain in the longitudinal cross-section of the sample in the vicinity of the basic shear zone, together with the distribution of contact surface tractions, for four values $\mu = 0.01, 0.1, 0.2, 0.3$ of the assumed Coulomb friction coefficient. It has been found that while the value of μ does not influence the strain distribution except in the surface layer, it affects the length of the outer corner gap identified as a zone where the surface tractions are zero.

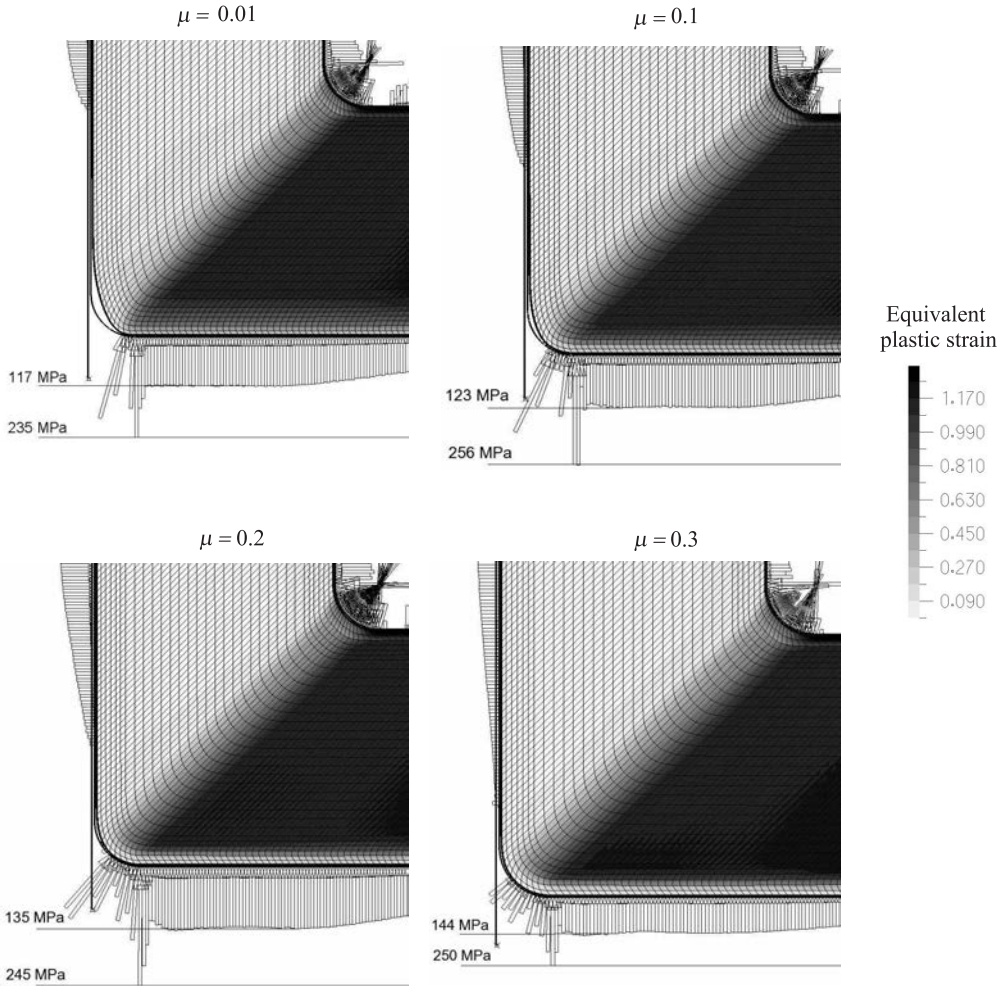


FIG. 15. Distribution of equivalent plastic strain and of surface tractions during the first pass through Die I, for different values $\mu = 0.01, 0.1, 0.2, 0.3$ of the Coulomb friction coefficient. The development of the corner gap is dependent on the friction conditions.

In Fig. 16a the force acting on the punch during the first and second pass, using Die I for route C, is plotted versus the punch displacement for different values of the Coulomb friction coefficient. In Fig. 16b the respective distributions of equivalent plastic strain across the billet are presented. The forming force grows with increasing friction coefficient as expected, whereas the distributions of equivalent plastic strain are very similar for different friction coefficients. Small differences in the sub-surface layers of the billet are only observed.

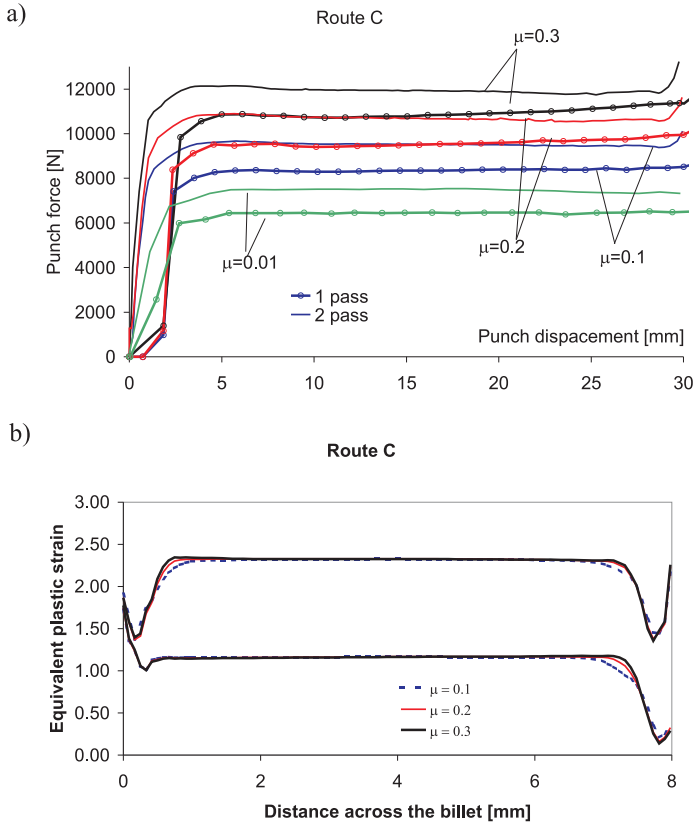


FIG. 16. Simulation results for ECAP Route *C* using Die I for different values $\mu = 0.1, 0.2, 0.3$ of the Coulomb friction coefficient, a) force acting on the punch versus the punch displacement, b) distribution of equivalent plastic strain across the billet.

In Fig. 17 the longitudinal distribution of equivalent plastic strain after the first pass through the ECAP Dies I and II is shown first, followed by similar pictures after the second pass according to routes *A* and *C*. It can be seen that the strain distribution is more non-uniform after the second pass for route *A* than that for *C*, which is more clearly visible for Die I. In turn, the distribution of equivalent plastic strain is found more uniform for Die I with $\psi = 0^\circ$ than that for Die II with $\psi = 20^\circ$. During a passage through Die II, a less deformed layer is formed in the lower part of the sample. After a closer look at the deformed mesh, a conclusion can be drawn that this is due to formation of a rotating and less deforming zone, in vicinity of the rounded outer corner of Die II. The obtained results are in qualitative agreement with previous studies [9, 11, 20, 28, 29]. A more detailed plots of the distributions of equivalent plastic strain across the material sample are shown in Fig. 18.

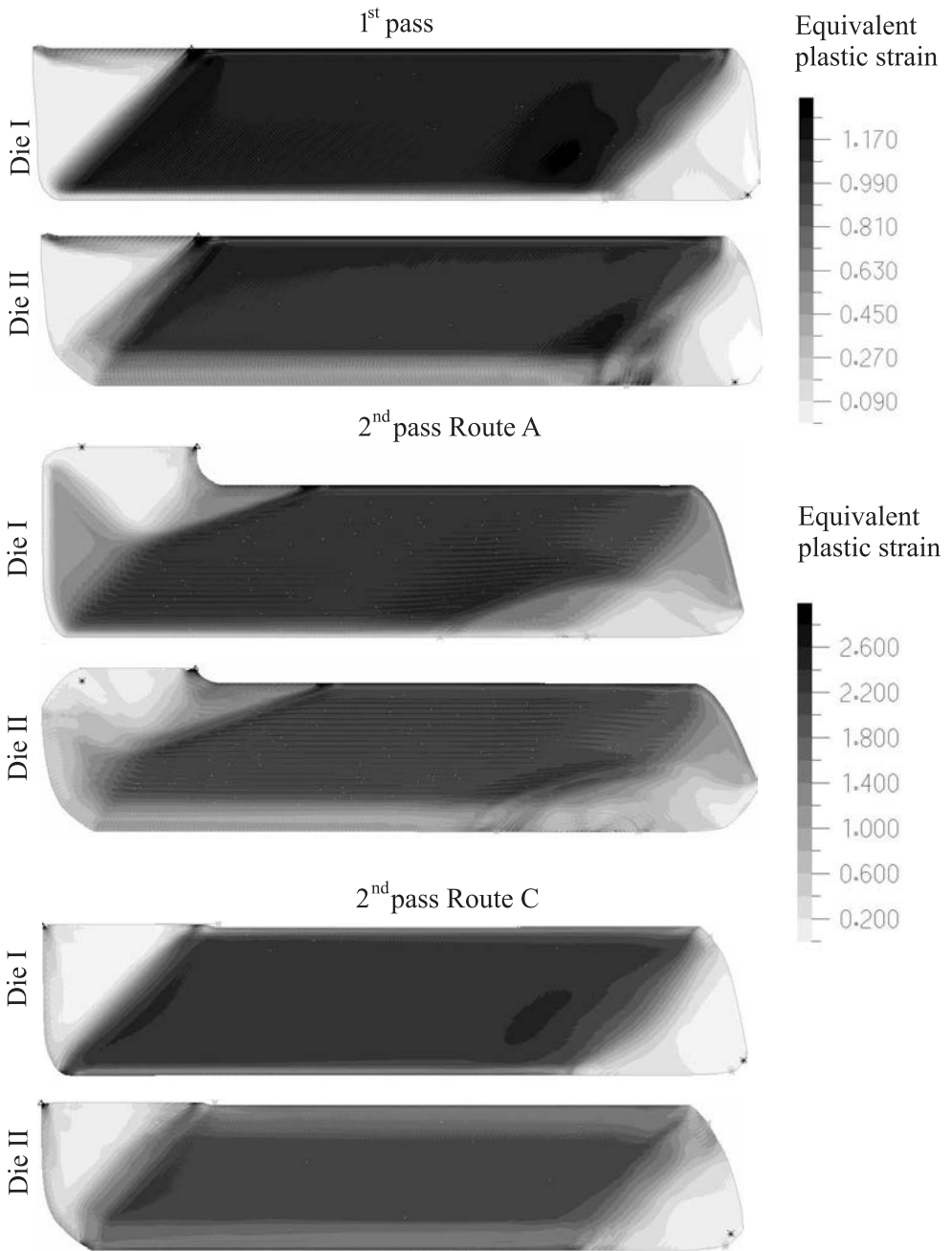


FIG. 17. The fields of equivalent plastic strain during ECAP, after the first and second pass through Die I and II for routes A and C.

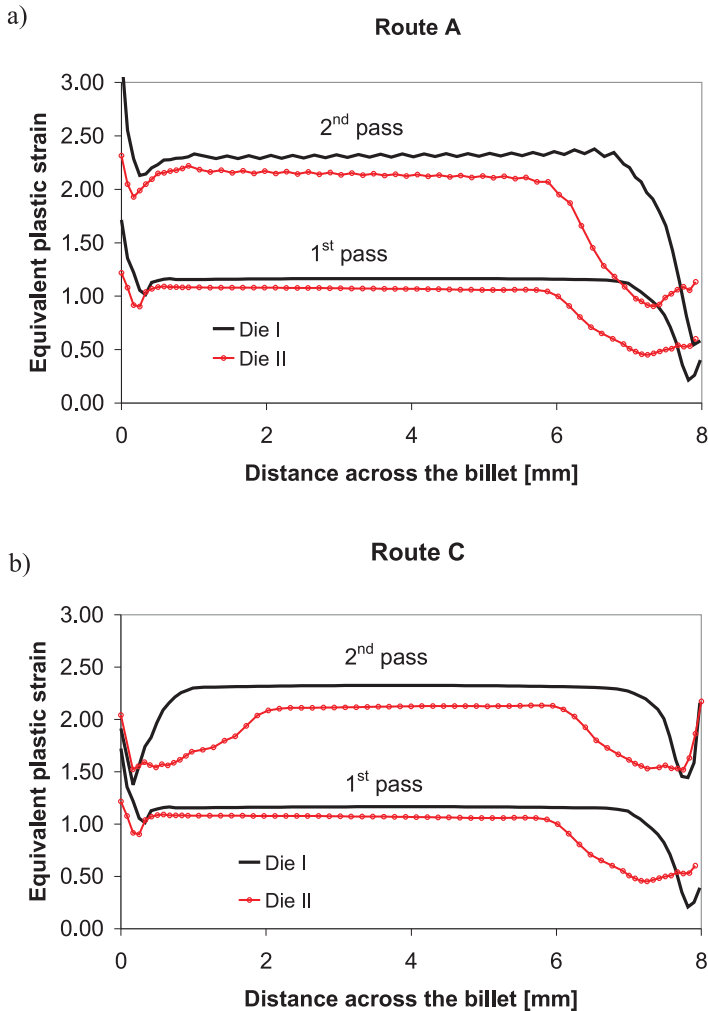


FIG. 18. Distribution of equivalent plastic strain across the billet during ECAP, after the first and second pass through Dies I and II, for routes A and C.

The difference between the deformation fields calculated for isotropic hardening and for kinematic hardening, corresponding to the same stress-strain curve for monotonic loading and for the same ECAP conditions, has not been found to be significant. A more essential and expected difference appears between the plots of the total force acting on the punch during the second pass according to route C, cf. Fig. 19. The reason for the difference is clear as for this route the direction of shear is reversed, which corresponds to the decrease of the shear stress when kinematic rather than isotropic hardening is assumed.

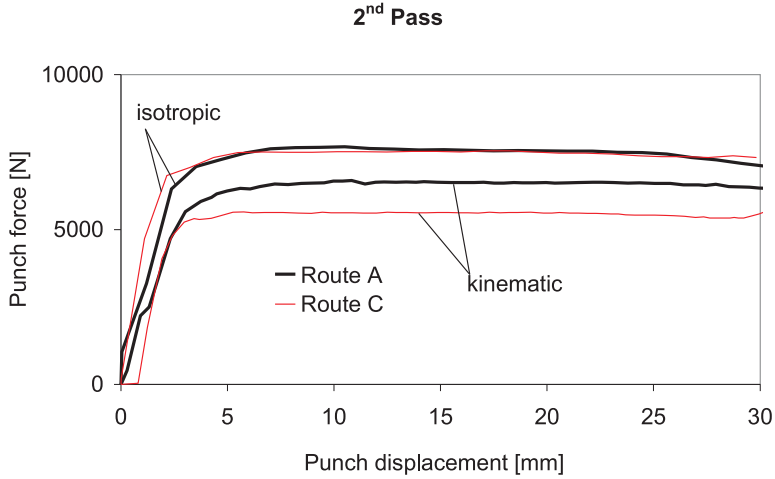


FIG. 19. Force acting on the punch versus the punch displacement during the second pass of ECAP, using Die II with negligible friction ($\mu = 0.01$). The results are for routes A and C and for either isotropic or kinematic hardening.

4. CONCLUSIONS

Finite Element Method simulations of the CEC and ECAP processes have been carried out for the elastoplastic material with strain hardening under isothermal conditions. The model parameters were calibrated for polycrystalline pure aluminium (99.99%) at room temperature.

The CEC process was simulated for various die shape parameters: ratio d_0/d_m (of diameters of the chambers and central cylindrical channel of the die, respectively), α (inclination angle of conical parts that connect chambers with the channel) and a (length of the cylindrical channel). The diameter ratio d_0/d_m is the most important parameter which determines the overall magnitude of strain in a single pass. The simulations performed have shown that the deformation is always non-uniform, with a peak near the outer radius of the sample. However, the degree of non-uniformity, defined as the ratio of maximum to minimum equivalent strain along the sample radius, is found to depend strongly on the value of d_0/d_m .

For dies with diameter ratio 10/9.5 and 10/9 the accumulated equivalent strain near the sample axis is much less than the theoretical value for uniform deformation, and the degree of non-uniformity is large and increases with subsequent cycles. If the diameter ratio d_0/d_m is too small then the plastic strain accumulation in the inner part may even be suspended, as it happened for the die 10/9.5 with the other parameters provided in Fig. 12. With the increase of the

diameter ratio the deformation becomes more uniform, and for diameter ratio 10/8 the degree of non-uniformity equal to 1.7 does not increase after subsequent cycles. Equivalent plastic strain distribution is found to be fairly uniform for somewhat higher diameter ratio (15/11), with the degree of non-uniformity reduced to 1.2. The above conclusions have been drawn using the conventional plasticity model which does not describe formation of macroscopic shear bands observed experimentally.

The angle of inclination of conical parts of the die has also a significant influence on the resulting homogeneity of the sample, and with the angle growth the non-homogeneity increases. By decreasing the inclination angle at a fixed value of d_0/d_m , homogeneity of the deformation can be substantially improved. The influence of length a of the central cylindrical channel of the die is less substantial.

Friction on the material/tool contact surface has a considerable influence on the strain peak near the outer surface being in contact with the tool, whereas in central part the deformation it is found to be only slightly affected by friction.

Finite Element simulations of two passes of the ECAP process were carried out for routes A and C using two die shapes and for different friction conditions.

It is found that the value of the Coulomb friction coefficient μ does not influence the strain distribution except in the sub-surface layers, although the value of μ affects the length of the outer corner gap identified as a zone where the surface tractions are zero.

A uniform region of equivalent plastic strain accumulated in the first and second pass of ECAP is obtained in the central part of the billet. The strain distribution after the second pass is more non-uniform for route A than for route C, especially for Die I. In turn, the distribution of equivalent plastic strain is found to be more uniform for Die I with $\psi = 0^\circ$ than for Die II with $\psi = 20^\circ$. During a passage through Die II, a less deformed layer is formed near the outer corner of the die.

ACKNOWLEDGMENT

This work has been supported by the State Committee for Scientific Research (KBN) in Poland through Grant No. PBZ-KBN-096/T08/2003.

REFERENCES

1. V.M. SEGAL, *Materials processing by simple shear*, Mater. Sci. Eng. A, **197**, 157–164, 1995.
2. R.Z. VALIEV, T.G. LANGDON, *Principles of equal-channel angular pressing as a processing tool for grain refinement*, Progress in Materials Science, **51**, 881–981, 2006.

3. J. RICHERT, M. RICHERT, *A new method for unlimited deformation of metals and alloys*, Aluminium, **8**, 604–607, 1986.
4. M. RICHERT, A. KORBEL, *The Effect of strain localization on mechanical properties of Al99,992 in the range of large deformations*, J. Mater. Proc. Technol., **53**, 331–340, 1995.
5. M. RICHERT, J. RICHERT, J. ZASADZINSKI, H. DYBIEC, *The boundary strain hardening of aluminium with unlimited cumulation of large deformation*, Z. Metallkd., **79**, 741, 1988.
6. M. RICHERT, Q. LIU, N. HANSEN, *Microstructural evolution over a large strain range in aluminium deformed by cyclic extrusion–compression*, Materials Science and Engineering A, **260**, 275–283, 1999.
7. M. RICHERT, H.P. STUWE, M.J. ZEHETBAUER, J. RICHERT, R. PIPPAN, CH. MOTZ, E. SCHAFLENER, *Work hardening and microstructure of AlMg5 after severe plastic deformation by cyclic extrusion and compression*, Materials Science and Engineering A, **355**, 180–185, 2003.
8. L. DUPUY, E.F. RAUCH, *Deformation paths related to equal channel angular extrusion*, Materials Science and Engineering A, **337**, 241–247, 2002.
9. I. J. BEYERLEIN, C. N. TOME, *Analytical modeling of material flow in equal channel angular extrusion (ECAE)*, Materials Science and Engineering A, **380**, 171–190, 2004.
10. C. LIU, D.J. ALEXANDER, *A kinematic analysis of the angular extrusion (AE) operations* Materials Science and Engineering A, **391**, 198–209, 2005.
11. V.M. SEGAL, *Equal channel angular extrusion: from macromechanics to structure formation*, Materials Science and Engineering A, **271**, 322–333, 1999.
12. V.M. SEGAL, *Slip line solutions, deformation mode and loading history during equal channel angular extrusion*, Materials Science and Engineering A **345**, 36–46, 2003.
13. J. ALKORTA, J.G. SEVILLANO, *A comparison of FEM and upper-bound type analysis of equal-channel angular pressing (ECAP)*, Journal of Materials Processing Technology, **141**, 313–318, 2003.
14. B.S. ALTAN, G. PURCEK, I. MISKIOGLU, *An upper-bound analysis for equal-channel angular extrusion*, Journal of Materials Processing Technology, **168**, 137–146, 2005.
15. P.B. PRANGNELL, C. HARRIS, S.M. ROBERTS, *Finite element modelling of equal-channel angular extrusion*, Scripta Mater., **37**, 983–989, 1997.
16. H.S. KIM, M.H. SEO, S.I. HONG, *On the die corner gap formation in equal channel angular pressing*, Materials Science and Engineering A, **291**, 86–90, 2000.
17. A. ROSOCHOWSKI, R. RODIET, P. LIPÍŃSKI, *Finite element simulation of cyclic extrusion-compression*, Metal Forming 2000, PIETRZYK *et al.* [Eds.], 253–259, 2000.
18. A. ROSOCHOWSKI, L. OLEJNIK, *Numerical and physical modelling of plastic deformation in 2-turn equal channel angular extrusion*, Journal of Materials Processing Technology, **125–126**, 309–31, 2002.
19. C.J. LUIS PÉREZ, P. GONZÁLEZ, Y. GARCÉS, *Equal channel angular extrusion in a commercial Al–Mn alloy*, Journal of Materials Processing Technology, **143–144**, 506–511, 2003.
20. S. LI, M.A.M. BOURKE, I.J. BEYERLEIN, D.J. ALEXANDER, B. CLAUSEN, *Finite element analysis of the plastic deformation zone and working load in equal channel angular extrusion*, Materials Science and Engineering A, **382**, 217–236, 2004.

21. F. YANG, A. SARAN, K. OKAZAKI, *Finite element simulation of equal channel angular extrusion*, Journal of Materials Processing Technology, **166**, 71–78, 2005.
22. R.K. ORUGANTI, P.R. SUBRAMANIAN, J.S. MARTE, M.F. GIGLIOTTI, S. AMANCHERLA, *Effect of friction, backpressure and strain rate sensitivity on material flow during equal channel angular extrusion*, Materials Science and Engineering A, **406**, 102–109, 2005.
23. A.V. NAGASEKHAR, YIP TICK-HON, S. LI, H.P. SEOW, *Stress and strain histories in equal channel angular extrusion/pressing*, Materials Science and Engineering A, **423**, 143–147, 2006.
24. ADINA R&D Inc. ADINA, *Theory and Modeling Guides*, Reports ARD 05–7, 2005.
25. N.Q. CHINH, J. ILLY, Z. HORITA, T. G. LANGDON, *Using the stress–strain relationships to propose regions of low and high temperature plastic deformation in aluminum*, Materials Science and Engineering A, **410–411**, 234–238, 2005.
26. Y. IWAHASHI, Z. HORITA, M. NEMOTO, T.G. LANGDON, *Factors influencing the equilibrium grain size in equal-channel angular pressing: Role of Mg additions to aluminum*, Metall. Mater. Trans., **29A**, 2503–2510, 1998.
27. S. KOMURA, Z. HORITA, M. NEMOTO, T.G. LANGDON, *Influence of stacking fault energy on the development of microstructure in equal-channel angular pressing*, Journal of Materials Research, **14**, 4044–4050, 1999.
28. A.V. NAGASEKHAR, T.H. YIP, *Optimal tool angles for equal channel angular extrusion of strain hardening materials by finite element analysis*, Computat Mater. Sci., 489–495, 2004.
29. J.R. BOWEN, A. GHOLINIA, S.M. ROBERTS, P.B. PRANGNELL, *Analysis of the billet deformation behaviour in equal channel angular extrusion*, Materials Science and Engineering A, **287**, 87–97, 2000.

Received October 25, 2006; revised version January 16, 2007.
